# Performance Improvement of the Droop Control for Single-Phase Inverters

Gustavo M. S. Azevedo[1], Marcelo C. Cavalcanti[1], Francisco A. S. Neves[1],
Pedro Rodriguez[2], Joan Rocabert[2]
[1]Federal University of Pernambuco (UFPE) - Department of Electrical Engineering, Recife, Brazil
[2]Polytechnical University of Catalunya (UPC) - Department of Electrical Engineering, Barcelona, Spain

***Abstract*—The droop control uses the local average values of the active and reactive power components for sharing the load power demand among inverters in parallel. In this paper, a method that uses a virtual quadrature reference frame to calculate the average power components injected by single-phase inverters is presented. This method improves the dynamic response of the power sharing control, as well as, completely eliminates the double frequency oscillation over the voltage and frequency synthesized by the inverter in steady state. Moreover, it is able to deal with nonlinear loads since the harmonic components that appears in the instantaneous power are filtered. The method is compared with the classical method, which is based on low pass filters, through simulation carried out in Matlab/Simulink and experimental results.**

## I. Introduction

Distributed generation (DG) system is emerging as a complementary structure to the traditional central power plants. This structure is constructed on the basis of decentralized generation of electricity close to consumption sites using DG sources [1]. The DG concept is especially promising when renewable energy resources are available and the environmental aspects have been contributed for its growth. The increase in DG penetration and the presence of multiple DG units have brought the new concept of microgrid (MG) [2]. In this concept, a MG is composed by a set of loads, generator and storage micro-units, distributed in a defined area, operating as an unique system, that can be connected to the main electric grid. In this kind of structure, it is necessary to connect many voltage sources in parallel, requiring control techniques capable of avoiding current circulation among the sources and sharing the load power. Besides, most of these sources have power electronics converters as interface between the primary energy source and the MG.

In this sense, the parallel operation of the DG units is a key feature in the MG. Nevertheless, the parallel operation of power inverters has been studied for a long time [3][4]. Initially, it was applied in uninterruptible power system to increase its power capability and reliability [5]. After that, it has been extensively applied to the DG systems and, recently, to the MG. There are many control techniques to perform the parallel operation of inverters, but the droop control method (DCM) is the most common. This method consists in emulating the behavior of large power generators, which droop their frequency when the delivered power increases [6]. The main feature of the DCM is that it does not use any physical communication among the inverters. Each inverter has its own controller that uses only its output information signals. However, the DCM has slow dynamic response since it requires low-pass filter (LPF) to compute the average power components [6][7]. Moreover, the double frequency oscillation, inherent to the single-phase instantaneous power, is not completely attenuated by the LPF and it appears in the inverter output voltage and frequency. The method proposed in [8] to calculate the power components of single-phase systems can overcome the aforementioned problems. This method uses a virtual quadrature reference frame to calculate the average power components injected by single-phase inverters.

This paper points out the characteristics of both aforementioned methods to calculate the power components and makes a comparison between them. Simulation and experimental results are provided to confirm the statements. Besides, the DCM is briefly presented as well as the inverter control strategy used in this work.

## II. Droop Control Method

The DCM uses the same principle of power electric systems. The inverters are controlled in such a way to present active power-frequency ($P$-$\omega$) and reactive power-voltage ($Q$-$V$) characteristics similar to a synchronous machine. Therefore, it is possible to connect many inverters in parallel to share the load power.

The power components between two bars, connected through an impedance $\mathbf{Z}$, as shown in Fig. 1, are given by

$$P = \frac{V_1^2}{Z}\cos\theta - \frac{V_1 V_2}{Z}\cos(\theta+\delta) \tag{1}$$

$$Q = \frac{V_1^2}{Z}\sin\theta - \frac{V_1 V_2}{Z}\sin(\theta+\delta). \tag{2}$$

If $X \gg R$, it can be assumed that the impedance has only inductive reactance, i.e., $\mathbf{Z} = X\angle 90^\circ$, and considering small values of $\delta$, (1) and (2) can be approximated by

$$P \cong \frac{V_1 V_2}{X}\delta \tag{3}$$

$$Q \cong \frac{V_1}{X}(V_1 - V_2), \tag{4}$$

These equations show that the active power depends predominantly of the power angle $\delta$ and the reactive power predominantly of the voltage difference $(V_1 - V_2)$, demonstrating the

978-1-4244-9312-8/11/$26.00 ©2011 IEEE

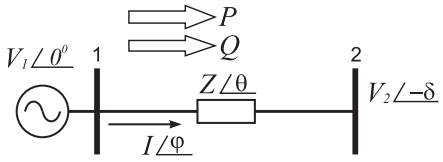


Fig. 1. Power between two bars.

relation $P$-$\delta$ and $Q$-$V$. In a practical situation, the dynamic control of frequency is used to impose the power angle and consequently the active power. Therefore, there is a relation between active power and frequency. These conclusions are the basis of the droop regulation of frequency and voltage through the active and reactive powers, respectively:

$$\omega = \omega_0 - D_p P \quad (5)$$

$$V = V_0 - D_q Q, \quad (6)$$

where $\omega_0$ and $V_0$ are the frequency and amplitude of the voltage without load and $D_p$ and $D_q$ are the droop coefficients of frequency and amplitude, respectively. Using the frequency $\omega$ instead of the angle $\delta$ is more adequate because in control techniques for inverters in parallel, one unit does not know the initial phase of the others. However, the initial frequency without load can be easily fixed as $\omega_0$ [6].

The previous analysis considers an inductive line. However, the low voltage grid is usually more resistive and consequently the characteristic (3) and (4) fails. In this case, a virtual inductance in the inverter output to ensure inductive behavior [6][9] can be used. In fact, the proper choice of this virtual inductance can also mitigate the line impedance unbalance, which occurs due to the unequal cables lengths [10].

## III. Inverter Control Design

Figure 2 shows the power stage of a single-phase inverter and its control diagram. The inverter consists of a full-bridge configuration and an output $LC$ filter. The equations that describe the large-signal dynamic behavior of this converter are

$$L\frac{di_L}{dt} = v_i - v_o - r_L i_L \quad (7)$$

$$C\frac{dv_o}{dt} = i_c = i_L - i_o, \quad (8)$$

where $r_L$ is the equivalent series resistance of the filter inductor, $v_i$ represents the average value of the inverter output voltage in one switching cycle, $v_o$ and $i_o$ are the output voltage and current, $i_L$ and $i_c$ are the currents through the filter inductor and capacitor, respectively.

The inverter output voltage can be controlled through $i_L$, as shown in (8). Moreover, this current can be controlled by the voltage $v_i$, imposed by the states of the inverter switches through a pulse-width modulator (PWM). Thus, two control loops are used to regulate the output voltage. The inner loop regulates the current $i_L$ and the outer loop regulates the output voltage, $v_o$. Besides, a feedforward is used to improve the dynamic response of the voltage controller. The control variable of $v_o$ is the inductor current and $i_o$ appears as a perturbation. This perturbation can be properly compensated by adding the measured value of $i_o$ to the voltage controller, $G_v(s)$. The controlled variables are sinusoidal and the proportional-resonant (PR) controller is a suitable choice to implement the regulation loops [11]. The transfer functions for the current and voltage controllers are given by

$$G_I(s) = k_{p_I} + k_{r_I}\frac{s}{s^2+\omega^2} \quad (9)$$

$$G_V(s) = k_{p_V} + k_{r_V}\frac{s}{s^2+\omega^2}, \quad (10)$$

where $k_p$ and $k_r$ are the proportional and resonant gains, the index $I$ and $V$ represent the current and voltage controllers, and $\omega$ is the resonant frequency of the controller, which must coincide with the controlled signal frequency.

The bandwidth of the inner loop was chosen ten times larger than the outer voltage loop in order to decouple their dynamics. Table I shows the inverter and controller parameters used in the system. With these parameters the bandwidth of the current loop is around $3.2kHz$ and the bandwidth of the voltage loop is around $340Hz$ .

The other control loop in the system of Fig. 2 is the virtual impedance. The virtual output impedance loop is able to fix the output impedance of the inverter by subtracting a processed part of the output current $i_o$ to the voltage reference of the inverter $e^*$ [12]. The output impedance of the closed-loop inverter affects the power sharing accuracy and determines the $P$-$Q$ DCM. Furthermore, the proper design of this impedance can reduce the impact of the line-impedance unbalance [10]. The DCM assumes that the line impedance is inductive, but the low voltage systems are generally resistive. Therefore, selecting the virtual impedance as inductive and higher than the line resistance ensures the proper load sharing.

On the other hand, the inductive-effect of the inverter output increases the voltage total harmonic distortion (THD) when supplying nonlinear loads due to the frequency dependency of the inverter output-reactance value. To overcome this drawback the function $F(s)$ (Fig. 2) uses a high-pass filter instead of a pure derivative term [13]. Thus, the virtual impedance is obtained through

$$v_o^* = e^* - L_V\frac{\omega_c s}{s+\omega_c}, \quad (11)$$

TABLE I
Parameters of the inverter and controller system.

| Parameter | Symbol | Value |
|---|---|---|
| Filter inductor | $L$ | $1\,mH$ |
| Filter inductor resistance | $r_L$ | $0.2\,\Omega$ |
| Filter capacitor | $C$ | $20\,\mu F$ |
| Current proportional gain | $k_{p_I}$ | 20 |
| Current resonant gain | $k_{r_I}$ | 200 |
| Voltage proportional gain | $k_{p_V}$ | 0.05 |
| Voltage resonant gain | $k_{r_V}$ | 5 |
| Resonant frequency | $\omega$ | $2\pi\,60\,rad/s$ |

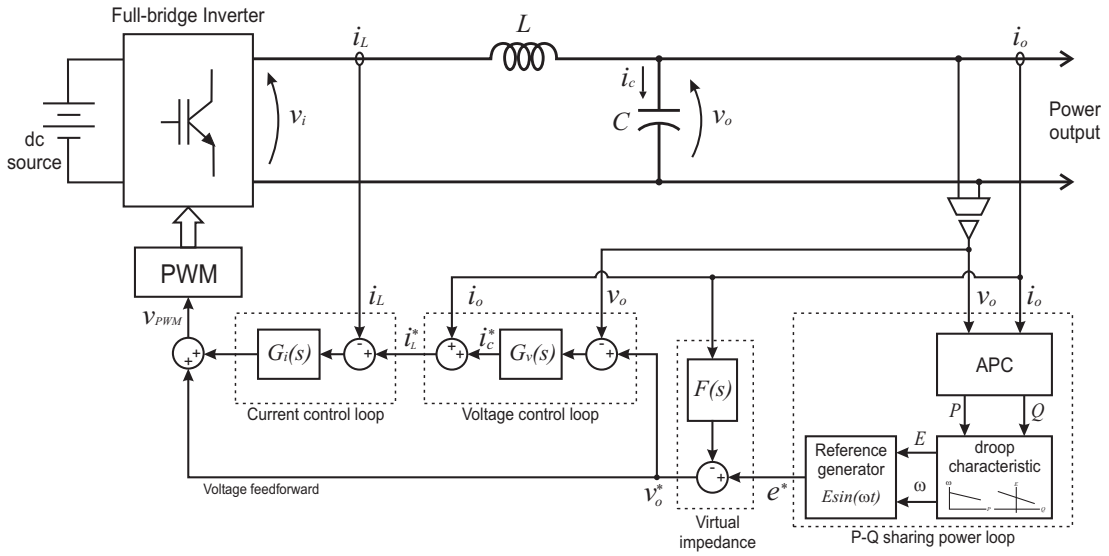


Fig. 2. Power stage of the single-phase inverter and its control block diagram.

where $L_V$ is the virtual inductor value and $\omega_c$ is the cutoff frequency of the high-pass filter.

The last control loop in Fig. 2 is the active and reactive power sharing loop which has three blocks: the average power calculator (APC) used to compute the average value of the active and reactive powers; the droop characteristic to perform the proper power sharing; and the voltage reference generator based on the droop characteristic.

The power dynamic is defined by the LPF used in the APC and the droop coeficientes of each inverter. Besides the effect on the system dynamic and stability, the APC has also effect on the output voltage quality. Consider the converter output voltage and current given by

$$v_o = \sqrt{2}V\cos(\omega t) \quad (12)$$

$$i_o = \sqrt{2}I\cos(\omega t - \phi), \quad (13)$$

respectively, where $V$ and $I$ are the voltage and current rms values and $\phi$ is the angle between current and voltage. The instantaneous active power delivered by the converter is

$$p = v_o\, i_o \quad (14)$$

$$p = \underbrace{VI\cos\phi}_{P} + \underbrace{VI\cos(2\omega t - \phi)}_{\tilde{p}} \quad (15)$$

and the reactive power is

$$q = v_{o_\perp}\, i_o \quad (16)$$

$$q = \underbrace{VI\sin\phi}_{Q} + \underbrace{VI\sin(2\omega t - \phi)}_{\tilde{q}} \quad (17)$$

where $v_{o_\perp}$ is the in quadrature output voltage.

From (15) and (17), it can be observed that the active and reactive powers have two components: one constant corresponding to the average value and the other oscillatory with double frequency. The average components correspond to the classic definition of power for steady state sinusoidal systems

$$P = VI\cos\phi \quad (18)$$

$$Q = VI\sin\phi. \quad (19)$$

The power control loops of the inverters operate on the average values, $P$ and $Q$. Therefore, it is necessary a method to extract these power components. Usually first order LPF are used [6][12][13]. Their cutoff frequency has to be very low to attenuate the power oscillating components, but this results in a slow dynamic response. The transfer function of a first order LPF with cutoff frequency $\omega_c$ is

$$F(s) = \frac{\omega_c}{\omega_c + s}, \quad (20)$$

where the settling time is given by $t_s = 4/\omega_c$. If $\omega_c$ is one decade lower than the fundamental frequency, $t_s = 106.10ms$. Thus, with a load step, the LPF output will take around six fundamental cycles to indicate the new value of load power. Considering the fundamental frequency $\omega_s$ and $\omega_c = 0.1\,\omega_s$, the first order LPF attenuation for the double frequency ($\omega = 2\omega_s$) component is $-26dB$ or $0.0499$. It means that the APC will indicate $P$, $Q$ and an oscillation with frequency $2\omega_s$ and amplitude of almost 5% of the load apparent power.

An improvement is achieved by replacing the first order LPF by a second order LPF, which the transfer function is

$$F(s) = \frac{\omega_n^2}{s^2 + 2\xi\omega_n s + \omega_n^2}, \quad (21)$$

where $\omega_n$ is the natural frequency without damping and $\xi$ is the damping factor. The settling time of this filter is $t_s = 4/(\xi\omega_n)$, for $0 < \xi < 1$. Thus, considering $\xi = 1/\sqrt{2}$ (Butterworth filter) and a $\omega_n$ that results in the same settling time of the first order LPF, the attenuation in (21) for the double frequency will be $0.5\%$, i.e., $20dB$ lower than the first order

LPF. It should be noted that this approach can not completely eliminate oscillating components in the average power.

## IV. Enhanced Average Power Calculator

Although the single-phase is a one-dimensional system, a virtual bi-dimensional and orthogonal frame can be achieved by [8]

$$\vec{v} = \begin{bmatrix} v_d \\ v_q \end{bmatrix} = \begin{bmatrix} v_o \\ v_{o_\perp} \end{bmatrix} \tag{22}$$

$$\vec{i} = \begin{bmatrix} i_d \\ i_q \end{bmatrix} = \begin{bmatrix} i_o \\ i_{o_\perp} \end{bmatrix}. \tag{23}$$

As in the three-wire three-phase system, the powers can be obtained by

$$\bar{p} = \frac{1}{2}\left(\vec{v}\cdot\vec{i}\right) = \frac{1}{2}\left(v_d\, i_d + v_q\, i_q\right) \tag{24}$$

$$\bar{q} = \frac{1}{2}\left|-\vec{v}\times\vec{i}\right| = \frac{1}{2}\left(v_q\, i_d - v_d\, i_q\right). \tag{25}$$

With the voltage and current given by (12) and (13), respectively, the power components, using (24) and (25), result in

$$\bar{p} = VI\cos\phi = P \tag{26}$$

$$\bar{q} = VI\sin\phi = Q. \tag{27}$$

It can be noted that this definition results in power components that differ from the instantaneous power that flows through the system. However, they are equivalent in average values. Therefore it results in an interesting way to substitute the APC based on LPF. In this work, this method is called enhanced APC (EAPC).

The quadrature signals are obtained using the structure presented in [14], where the settling time can be adjusted through a constant. This time must be chosen in order to assure the MG stability.

## V. Simulation and Experimental Results

The parallel operation of two single-phase inverters was simulated in Matlab/Simulink in order to compare the behavior of the APC methods. Each inverter is a full-bridge topology with switching frequency of $20kHz$ and a LC output filter, using the parameters listed in Table I and Table II. The inverters are fed by $400V$ $dc$ sources. The electrical scheme considered in this simulation is shown in Fig. 3. Inverters with different rated powers to demonstrate the proportional load sharing between them are considered. The line impedances, $Z_{L1}$ and $Z_{L2}$, are equal to $1 + j189\,m\Omega$. The loads, $L_1$ and $L_2$, have the same impedance $6.45 + j4.84\,\Omega$ that results in $1.2 + j0.9\,kVA$ when they are fed by a $110V$ source. The virtual impedance, at fundamental frequency, of the inverter $\#2$ is half of the inverter $\#1$ to improve the reactive power sharing.

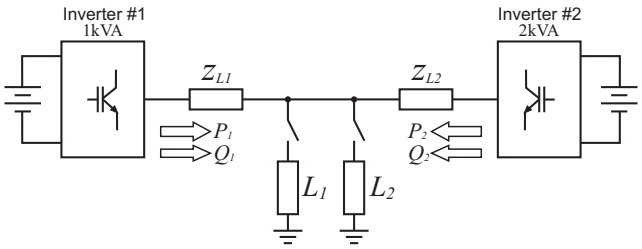


Fig. 3. Electrical scheme of inverters in parallel considered in simulation.

The voltage amplitude and frequency of the inverters 1 and 2 are shown in Fig. 4(a). First, there is no load connected to the system, $E_1 = E_1^*$, $E_2 = E_2^*$, $f_1 = f_1^*$ and $f_2 = f_2^*$. When the first load is connected (at $t = 0.5s$) the active powers increase and the frequencies droop. The same effect occurs with the reactive powers and the voltage amplitudes. At $t = 3s$, the load power has doubled and the voltage amplitude and frequency droop again. The power components delivered by each inverter are shown in Fig. 4(b). It can be noted that the active power is perfectly shared between the inverters, with the inverter $\#2$ delivering double power. There is also adequate sharing between the reactive powers. Figure 4 confirms that there is no oscillating components in the reference values, resulting in power components without oscillation. It is worth to note that the power components are zero at no load, confirming that there is no circulating current between the inverters.

A comparison between the APC and EAPC methods during

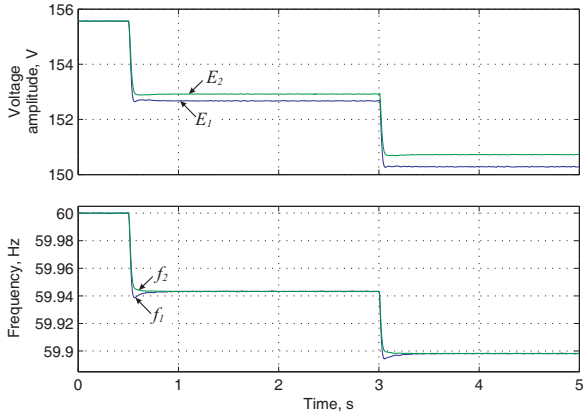


(a) References of the voltage amplitude and frequency.

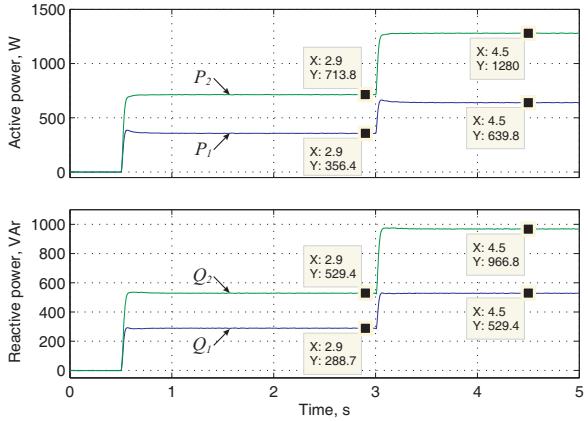


(b) Active and reactive powers supplied by the inverters.

Fig. 4. Simulation results of the proposed method for different load conditions.

a load transient is shown in Fig. 5. This transient occurs at $t = 3s$ when the other load, with the same power of the previous one, is added. The parameters of the EAPC are the same used before. The APC method uses 2nd order *Bessel* filter with cut-off frequency of $6Hz$ . For this method, cut-off frequencies higher than that, give rise to unstable conditions. The voltage amplitude and frequency of the inverter $\#2$ are shown in Fig. 5(a) for the both methods. The EAPC has faster dynamic response and does not have the double frequency oscillating component. These effects are reflected on the power components as shown in Fig. 5(b).

The EAPC robustness is evaluated in presence of distorted currents in Fig. 6. In this simulation the load $L_2$ is replaced by a typical rectifier. The current drawn by this load has the peak value of $16.5A$, crest factor of $2.05$ and THD of $67.4\%$. This nonlinear load is switched on at $t = 3s$. The inverters reference signals are shown in Fig. 6(a) and the power components delivered by each inverter are shown in Fig. 6(b). It should be noted that these values do not have oscillating components in steady state, even with the distorted current and the more oscillatory instantaneous power. In fact, the oscillating components in the instantaneous power have high frequency and they are easily filtered by the EAPC. The output voltage and current, for this case, are shown in Fig. 7.

The algorithms for power calculation based on APC and EAPC are implemented in a fixed-point DSP. The purpose here is only comparing these algorithms as a power measurer, i.e., they are not being used in a control loop. The APC and EAPC have the same parameters used in simulation. Figure 8 shows the experimental results of the classical APC and the EAPC for a load step. Note that the EAPC have faster dynamic response, converging to the final value in less than $50ms$, whereas the APC takes around $125ms$. The APC has double frequency oscillation, but it cannot be shown in these results due to the low resolution of the digital-to-analogic conversion system used in the prototype.

TABLE II
PARAMETERS OF THE SIMULATED SYSTEM.

| Parameter | Symbol | Value |
|---|---|---|
| Inverters nominal voltage | $V_n$ | $110V$ |
| Inverters nominal voltage frequency | $\omega_s$ | $2\pi 60\, Rad/s$ |
| Virtual inductance of inverter $\#1$ | $L_{V1}$ | $3\, mH$ |
| Virtual inductance of inverter $\#2$ | $L_{V2}$ | $1.5\, mH$ |
| Voltage droop of inverter $\#1$ | $n_1$ | $0.01\, V/VAr$ |
| Voltage droop of inverter $\#2$ | $n_2$ | $0.005\, V/VAr$ |
| Frequency droop of inverter $\#1$ | $m_1$ | $10^{-3}\, Rad\, W/s$ |
| Frequency droop of inverter $\#2$ | $m_2$ | $0.5\, 10^{-3}\, Rad\, W/s$ |

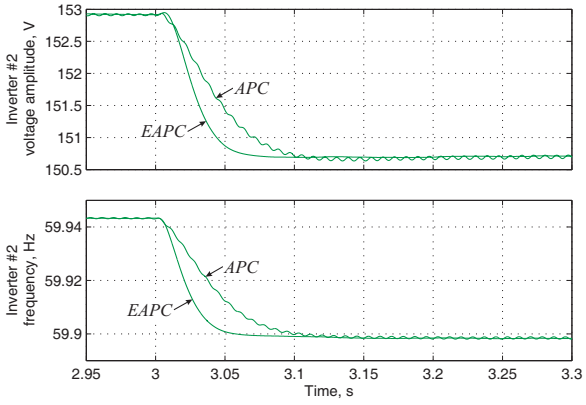


(a) References of the voltage amplitude and frequency for inverter #2.

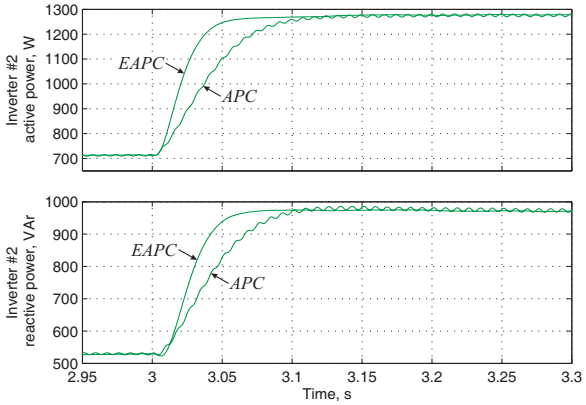


(b) Active and reactive powers supplied by the inverter #2.

Fig. 5. Comparison between the APC and EAPC methods during a load transient.

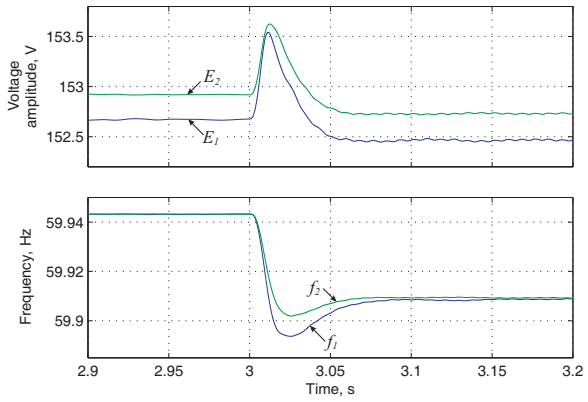


(a) References of the voltage amplitude and frequency.

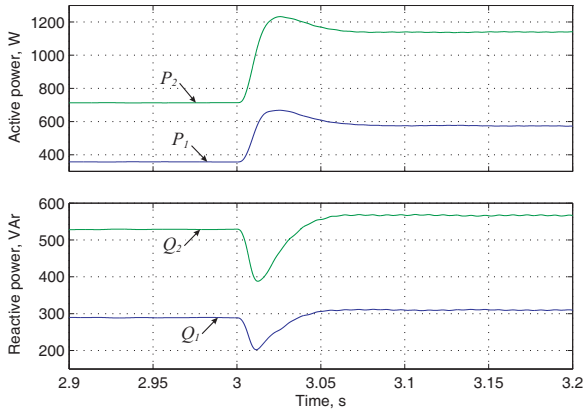


(b) Active and reactive powers supplied by the inverters.

Fig. 6. Performance of the EAPC method for nonlinear load.

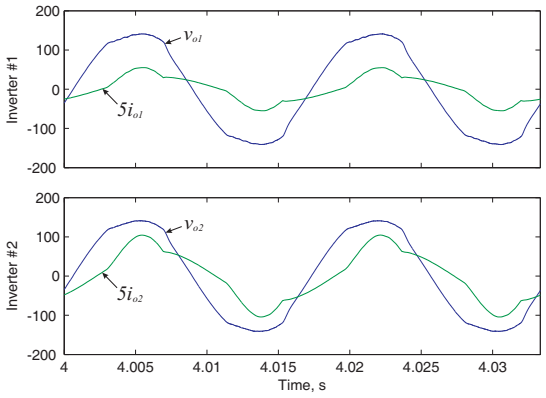


Fig. 7. Output voltages and currents of the inverter #1 and #2 when supplying both linear and nonlinear loads.

## VI. Conclusion

In this paper the droop control method and the problems regarding the extraction of the average values of the power components through low-pass filters are presented. A method to obtain these power components, called as enhanced average power calculator, is also discussed. This approach is based on a virtual quadrature reference frame. It improves the dynamic response of the power sharing control and eliminates the frequency oscillation in the voltage and frequency synthesized by the inverter, as shown in the comparative results.

## Acknowledgment

The authors would like to thank *Conselho Nacional de Desenvolvimento Científico e Tecnológico - CNPq* and *Coordenação de Aperfeiçoamento de Pessoal de Nível Superior - CAPES*, Brazil, and the project ENE2008-06841-C02-01/ALT, Spain, for the financial support.

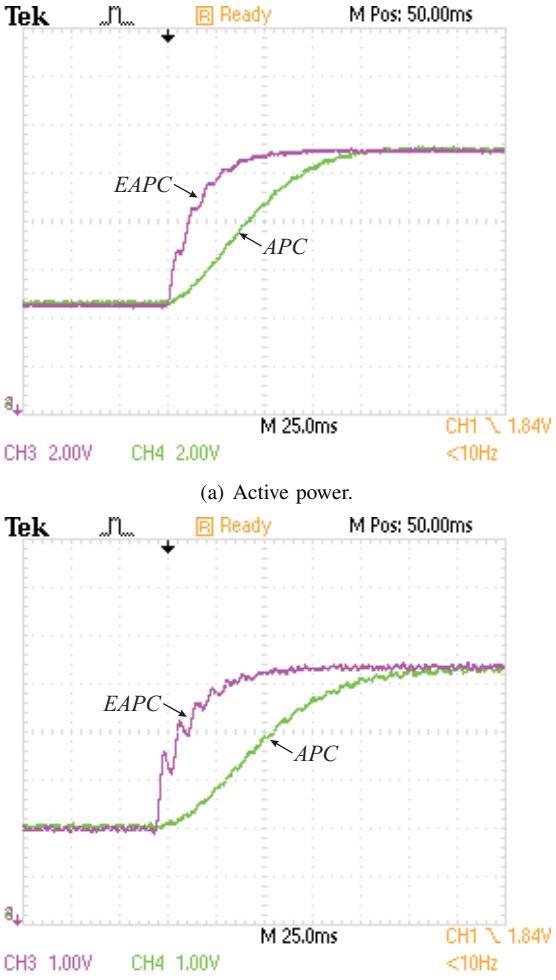


Fig. 8. Experimental results of the comparison between the classical APC and the EAPC.

## References

[1] F. Katiraei and M. Iravani, "Transients of a micro-grid system with multiple distributed energy resources," in *International Conference on Power Systems Transients*, june 2005, pp. 19–23.

[2] B. Lasseter, "Microgrids (distributed power generation)," in *IEEE Power Engineering Society Winter Meeting*, 2001.

[3] T. Kawabata and S. Higashino, "Parallel operation of voltage source inverters," *IEEE Trans. Ind. Appl.*, vol. 24, no. 2, pp. 281–287, 1988.

[4] A. Tuladhar, H. Jin, T. Unger, and K. Mauch, "Control of parallel inverters in distributed ac power systems with consideration of line impedance effect," *IEEE Trans. Ind. Appl.*, vol. 36, no. 1, pp. 131–138, jan/feb 2000.

[5] D. Shanxu, M. Yu, X. Jian, K. Yong, and C. Jian, "Parallel operation control technique of voltage source inverters in ups," in *International Conf. Power Electron. and Drive Systems*, vol. 2, 1999, pp. 883–887.

[6] J. M. Guerrero, J. Matas, L. G. de Vicuña, M. Castilla, and J. Miret, "Decentralized control for parallel operation of distributed generation inverters using resistive output impedance," *IEEE Trans. Ind. Electron.*, vol. 54, no. 2, pp. 994–1004, Apr. 2007.

[7] Y. Mohamed and E. El-Saadany, "Adaptive decentralized droop controller to preserve power sharing stability of paralleled inverters in distributed generation microgrids," *IEEE Trans. Power Electron.*, vol. 23, no. 6, pp. 2806–2816, 2008.

[8] B. Burger and A. Engler, "Fast signal conditioning in single phase systems," in *European Conference on Power Electronics and Applications*, 2001.

[9] K. D. Brabandere, B. Bolsens, J. V. den Keybus, A. Woyte, J. Driesen, and R. Belmans, "A voltage and frequency droop control method for parallel inverters," *IEEE Trans. Ind. Electron.*, vol. 22, no. 4, pp. 1107–1115, july 2007.

[10] I. Batarseh, K. Siri, and H. Lee, "Investigation of the output droop characteristics of parallel-connnected dc-dc converters," vol. 2, jun 1994, pp. 1342–1351.

[11] Y. Sato, T. Ishizuka, K. Nezu, and T. Kataoka, "A new control strategy for voltage-type pwm rectifiers to realize zero steady-state control error in input current," *IEEE Trans. Ind. Appl.*, vol. 34, no. 3, pp. 480–486, may/jun 1998.

[12] J. M. Guerrero, J. C. Vasquez, J. Matas, M. Castilla, and L. G. de Vicuña, "Control strategy for flexible microgrid based on parallel line-interactive ups systems," *IEEE Trans. Ind. Electron.*, vol. 56, no. 3, pp. 726–736, mar. 2009.

[13] J. M. Guerrero, L. G. de Vicuna, J. Matas, M. Castilla, and J. Miret, "A wireless controller to enhance dynamic performance of parallel inverters in distributed generation systems," *IEEE JPWRE*, vol. 19, no. 5, pp. 1205–1213, Sep. 2004.

[14] P. Rodriguez, R. Teodorescu, I. Candela, A. Timbus, M. Liserre, and F. Blaabjerg, "New positive-sequence voltage detector for grid synchronization of power converters under faulty grid conditions," in *Power Electronics Specialists Conference, PESC*, jun 2006, pp. 1–7.